Crystallization Behavior and Morphology of Biodegradable Polylactide/ Layered Silicate Nanocomposite

Joo Young Nam, Suprakas Sinha Ray, and Masami Okamoto*

Advanced Polymeric Materials Engineering, Graduate School of Engineering, Toyota Technological Institute, Hisakata 2-12-1, Tempaku, Nagoya 468 8511, Japan

Received May 13, 2003; Revised Manuscript Received July 27, 2003

ABSTRACT: An intercalated polylactide (PLA)/layered silicate nanocomposite was prepared by simple melt extrusion of PLA and organically modified montmorillonite. The detailed crystallization kinetics and morphology of neat PLA before and after nanocomposite preparation were studied by using polarized optical microscopy, light scattering, differential scanning calorimetric, and wide-angle X-ray diffraction analyses. The overall crystallization rate and spherulitic texture of pure PLA were strongly influenced in the presence of montmorillonite particles.

Introduction

Recently, demand for biodegradable polymers with excellent materials properties is said to be growing at a rapid rate. In this direction polylactide (PLA) is one of the most promising candidates because it is made from agriculture products and is readily biodegradable.[1] PLA is a linear aliphatic thermoplastic polyester. High-molecular-weight PLA is generally prepared by the ring-opening polymerization of lactide.[2] Lactide is a cyclic dimer prepared by the controlled depolymerization of lactic acid, which in turn is obtained by the fermentation of corn, sugar beat, etc.[1,3] PLA has good mechanical properties, thermal plasticity, and biocompatibility and is readily fabricated, thus being a promising polymer for various end-use applications.[4]

So, increasing realization of the various intrinsic properties of PLA, coupled with knowledge of how such properties can be improved to achieve the compatibility with thermoplastics processing, manufacturing, and end-use requirements, has fueled technological and commercial interest in PLA.

Of particular interest is recently developed nanocomposite technology consisting of a polymer and organically modified layered silicate (OMLS) because they often exhibit remarkably improved mechanical and various other properties as compared to those of virgin polymer.[5]

In our recent publications,[6−11] we have reported on the preparation, characterization, mechanical and various other materials properties, biodegradability, melt rheology, and finally foam processing of a series of PLA/OMLS nanocomposites. In all cases intrinsic properties of pure PLA were concurrently improved after nanocomposites preparation. But if we want to control the mechanical and various other properties of neat PLA before and after nanocomposites preparation, we have to know the crystallization behavior of PLA in detail and also how it is affected in the presence of clay particles.

The main objective of this paper is to understand the effect of clay particle on the crystallization kinetics and crystallite structure and morphology of neat PLA upon nanocomposite formation with OMLS.

* To whom correspondence should be addressed: Tel +81 52 809 1861; Fax +81 52 809 1864; e-mail okamoto@toyota-ti.ac.jp.

Table 1. Characteristic Parameters of Neat PLA and PLACN4

parameters	neat PLA	PLACN4
$M_w \times 10^{-3}$/g mol^{-1}	177	161
M_w/M_n	1.58	1.58
T_m/°C	168	169.8
T_g/°C	60	59.2
χ_c/%	36	49.1
d_{001}/nm[a]	-	3.18

[a] d_{001} for C_{18}-MMT is equal to 2.31 nm.

Experimental Section

Materials. PLA with D content of 1.1−1.7% was supplied by Unitika Co. Ltd., Japan, and was dried under vacuum at 60 °C and kept under dry nitrogen gas for 1 week prior to use. The organically modified montmorillonite (MMT) (C_{18}-MMT) used in this study was supplied by Nanocor Inc. and was synthesized by replacing Na^+ ions in MMT (cation exchange capacity (CEC) of 110 mequiv/100 g, thickness ≈ 1 nm, average length of 150−200 nm) with octadecylammonium cations (C_{18}) by ion exchange.

Nanocomposites Preparation. C_{18}-MMT (powder) and PLA (pellets) were first dry-mixed by shaking them in a bag. The mixture was then melt-extruded using a twin-screw extruder (PCM-30, Ikegai Machinery Co.) operated at 210 °C (screw speed = 100 rpm, feed rate = 120 g/min) to yield nanocomposite strands. The nanocomposite prepared with 4 wt % of C_{18}-MMT was denoted as PLACN4. The strands were palletized and dried under vacuum at 60 °C for 48 h to remove water.

Gel Permeation Chromatography (GPC). The weight-average (M_w) and number-average (M_n) molecular weights of neat PLA and PLACN4 were determined from GPC (LC-VP, Shimadzu Co.), using polystyrene standards for calibration and tetrahydrofuran (THF) as the carrier solvent at 40 °C with a flow rate of 0.5 mL/min. For the GPC measurements first PLA or PLACN4 was dissolved in chloroform and then diluted with THF.

GPC results of PLA in pure state or C_{18}-MMT filled system are presented in Table 1. As anticipated, the incorporation of C_{18}-MMT resulted in a reduction in the molecular weight of the PLA matrix. Decreased molecular weights of PLA in PLACN4 may be explained by either the shear mixing of PLA and C_{18}-MMT or the presence of ammonium salt, both resulting in a certain degree of hydrolysis of PLA matrix at high temperature.

Wide-Angle X-ray Diffraction (WAXD). WAXD analyses were performed for the C_{18}-MMT powder, neat PLA, and PLACN4 (last two samples were crystallized at 110 °C for 1.5 h) using an Mxlabo X-ray diffractometer (MAC Science Co.; 3

10.1021/ma034623j CCC: $25.00
Published on Web 08/26/2003

kW, graphite monochromator, Cu Kα radiation (λ_x = 0.154 nm), operated at 40 kV and 20 mA). Samples were scanned in fixed time mode with counting time of 2 s under a diffraction angle 2θ in the range 1°−30°.

Transmission Electron Microscopy (TEM). The nanoscale structure of PLACN4 was investigated by means of TEM (H-7100, Hitachi Co.), operating at an accelerating voltage of 100 kV. The ultrathin section (the edge of the sample sheet perpendicular to the compression mold) with a thickness of 100 nm was microtomed at −80 °C using a Reichert Ultra cut cryo-ultramicrotome without staining.

Differential Scanning Calorimetry (DSC). The crystallized specimens were characterized by using a temperature-modulated DSC (TA 2920; TA Instruments) at the heating rate of 5 °C/min with a heating/cooling cycle of the modulation period of 60 s and an amplitude of ±0.769 °C to determine the crystallization temperature (T_c), the melting temperature (T_m), and heat of fusion. The DSC was calibrated with indium before experiments.

For the measurement of degree of crystallinity (χ_c) prior to DSC analysis, the extra heat absorbed by the crystallites formed during heating had to be subtracted from the total endothermic heat flow due to the melting of the whole crystallites. This can be done according to the principles and procedures described in our previous paper.[12] By considering the melting enthalpy of 100% crystalline poly(L-lactide) as 93 J/g,[13] we have estimated the value of the χ_c of neat PLA and PLACN4; these values are also presented in Table 1.

Crystallization. The thin film (thickness ≈ 30 μm) was prepared by pressing the film between two cover glasses at 200 °C using a hot plate. After the specimen was hold at 200 °C for 5 min on hot plate (in order to remove the thermal history), it was quickly transferred into a hot stage (Linkam LK600PM, Linkam Scientific Instruments, Ltd.)[14] set at the desired T_c and crystallized until full solidification (confirmed from the kinetics of crystallization using a polarizing optical microscope). The crystallized specimens were characterized by using DSC and WAXD.

Rayleigh Scattering Photometry and Polarized Optical Microscopy. We have employed time-resolved light scattering (LS) photometry to estimate the overall crystallization rate and its kinetics of neat PLA and PLACN4. The thin sample of about 30 μm thickness was quickly transferred from the melt state to the Linkam hot stage, placed in the LS apparatus, and set at the predetermined temperature, and immediately after attaining the T_c, a time-resolved LS measurement was carried out in the temperature range 80−130 °C. It should be mentioned here that there was some time lag between putting the sample on the hot stage and switching on the computer to collect the data which is ∼10 s, sufficient for the equilibration of temperature. The one-dimensional photometer was equipped with a 38-channel photodiode (PDA: Hamamastu Photonics Co.) array, which facilitated the angular dependence of scattering angle (θ_{LS}) covered between 1.4° and 30°. The radiation of polarized He−Ne laser of 632.8 nm wavelengths was used vertically to the sample, and the scattering profile was observed at an azimuthal angle of 45° under H_v (cross-polarized) alignment. We also used a conventional Polaroid camera (camera length = 156 mm) to recover the scattering patterns on a photographic film with an exposure time of 1/60 s.[15] The photographs were taken after full solidification of the sample.

We also measured the spherulite growth rate of neat PLA and PLACN4 in the temperature range of 80−130 °C. For the measurement of linear growth rate the thin samples were crystallized on the Linkam hot stage mounted on a polarized optical microscope (POM) (Nikon OPTI-PHOTO2-POL), and the diameter of the developed spherulite was measured with time using a video recording system (Linkam RTVMS, Linkam Scientific Instruments, Ltd.). After complete crystallization, the samples were observed using POM and fitted with a color-sensitive plate to determine the sign of birefringence, and then photographs were taken. The details regarding POM observation can be found in our previous paper.[16]

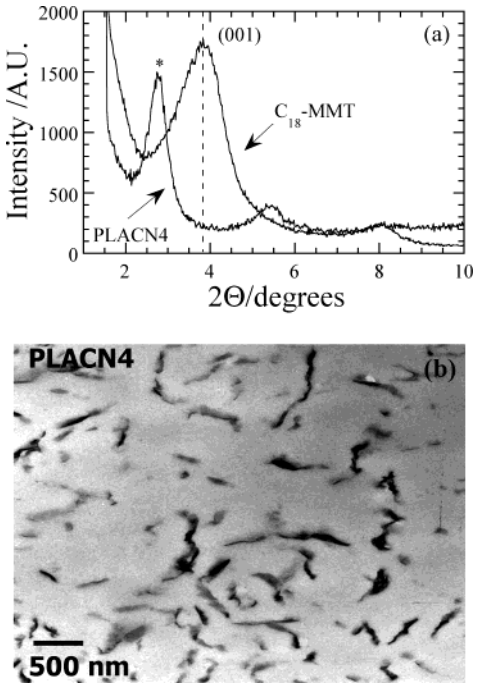

Figure 1. (a) WAXD patterns of C_{18}-MMT powder and PLACN4 sheet (crystallized at 110 °C for 1.5 h). The dashed line indicates the location of the silicate (001) reflection of C_{18}-MMT. The asterisk indicates the (001) peak for C_{18}-MMT dispersed in a PLA matrix. (b) High-resolution TEM bright field image of PLACN4. The dark entities are the cross section of the intercalated C_{18}-MMT layers, and the bright areas are the matrix.

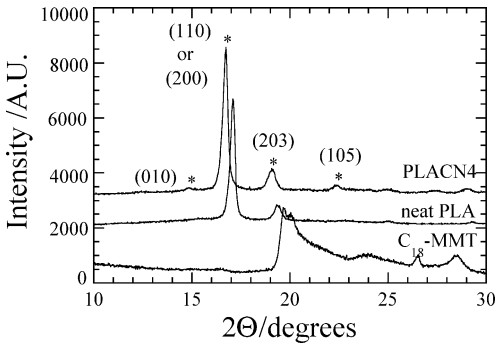

Figure 2. Typical WAXD patterns of pure PLA and PLACN4 samples crystallized at 110 °C for 1.5 h.

Results and Discussion

Nanocomposite Structure. The structure of the nanocomposite in the nanometer scale has typically been established using WAXD patterns and TEM observations. WAXD allows a direct evidence of the intercalation of polymer chains into the silicate galleries, whereas TEM offers a qualitative understanding of the internal structure through direct visualization. WAXD patterns of C_{18}-MMT powder and PLACN4 sheet (crystallized at 110 °C for 1.5 h) in the range 2θ = 1°−10° are presented in Figure 1a. Figure 1b shows bright-field TEM image of PLACN4. WAXD patterns and TEM observation established that a well-ordered intercalated nanocomposite was formed in the case of PLACN4. Details regarding the structural analysis can be found in our previous publications.[6,7]

Crystalline Structure. Figure 2 shows WAXD profiles of neat PLA and PLACN4 after crystallization at 110 °C for 1.5 h. The neat PLA exhibits a very strong reflection at 2θ = 17.1° due to diffraction from (200) and/

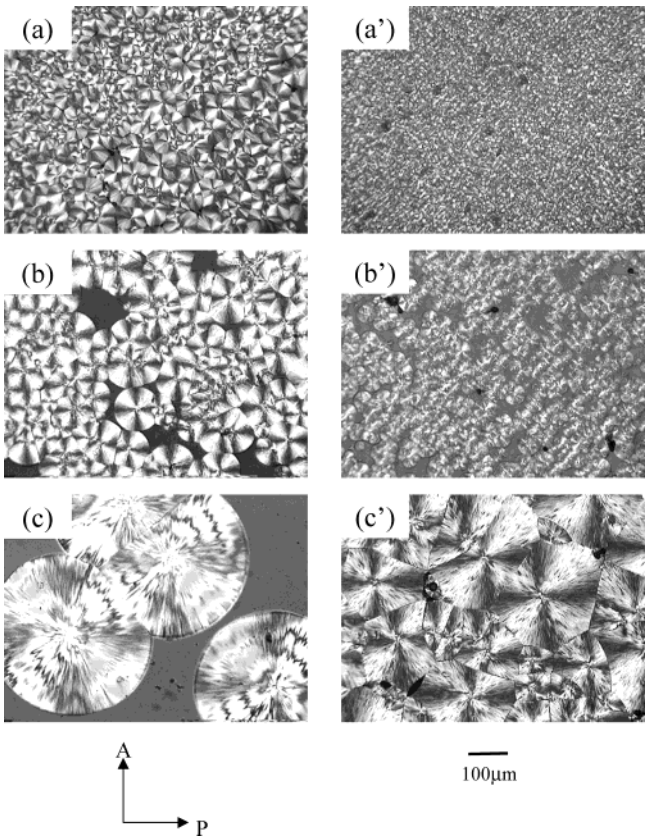

Figure 3. Optical micrographs of neat PLA (a−c) and PLACN4 (a′−c′) at various crystallization temperatures T_c: (a, a′) $T_c = 120$ °C; (b, b′) $T_c = 130$ °C; (c, c′) $T_c = 140$ °C.

or (110) planes and another reflection peak at $2\theta = 19.5°$ occurring from the (203) plane. On the other hand, in the case of PLACN4 these peaks are shifted toward the lower diffraction angle accompanied by another small peak at $2\theta = 15.3°$. After calculation, it was confirmed that this reflection is due to the (010) diffraction plane. These profiles indicate neat PLA crystals are the typical orthorhombic crystal;[17,18] however, the PLACN4 sample crystallized in a defect-ridden crystalline form. This unstable growth of crystallites of PLA in the presence of MMT particles may be due to the intercalation of PLA chains into the silicate galleries.

Spherulitic Texture. Figure 3 represents the POM observation of neat PLA and PLACN4 with a range of isothermal T_c. As shown in the figure, the spherulites are formed for both neat PLA and PLACN4 after isothermal crystallization, and spherulite sizes are systematically increases with increasing T_c. In the case of neat PLA, spherulites exhibited negative birefringence and high ordered spherulitic texture. At $T_c = 140$ °C, pure PLA formed very high ordered and ringed spherulites, but the ordering of PLACN4 spherulites is lower than that of neat PLA spherulites. The decrease of spherulitic size with the addition of C_{18}-MMT is clearly observed at $T_c = 120-140$ °C. At low T_c (≤120 °C), the size of spherulites is small and out of the range for the POM experiment. For this reason, we have employed LS in order to understand the spherulitic structure of the samples crystallized at low T_c.

Figure 4 shows the change in the H_v LS patterns after the isothermal crystallization of neat PLA and PLACN4 at $T_c = 90-120$ °C. A four-leaf-clover type pattern was clearly observed under H_v mode for neat PLA at all of the T_c after isothermal crystallization on that T_c for 5 h (Figure 4a−d). The one-dimensional H_v scattering profiles at an azimuthal angle of 45° in the scattering patterns of Figure 4 has a maximum at scattering angle θ_{LS}. The θ_{LS} is related to the average radius of the spherulite, R_s, as[19,20]

$$4.09 = 4\pi(R_s/\lambda_{LS}) \sin(\theta_{LS}/2) \quad (1)$$

where λ_{LS} is the wavelengths of the light used in LS measurement. Hence, the θ_{LS} is expected to become smaller when the R_s becomes larger. As shown in Figure 5, the R_s calculated from a maximum scattering angle becomes smaller with the addition of C_{18}-MMT. This result shows that the dispersed MMT particles act as a nucleating agent, which is evident from the increase in the number of density of nuclei causing smaller spherulite formation.

On the other hand, the diffused clover pattern was clearly observed for PLACN4 (Figure 4a′−d′) as compared to that of neat PLA. These results suggest that high ordered spherulites, where crystallites are regularly arranged along the radial direction within the spherulite, are formed for pure PLA, while ordering of spherulites for PLACN4 is lower than that of pure PLA.[21] This may be due to the originating of irregular orientation of lamella by the dispersed MMT particles inside the spherulites.

Crystallization Kinetics. To understand the crystallization kinetics of neat PLA before and after nanocomposite preparation at low T_c (≤120 °C), we have used time-resolved LS photometry, which is a powerful tool for estimating the overall crystallization rate and its kinetics in supercooled crystalline polymer liquid.[15] For the kinetics of crystallization, we can employ the integrated scattering intensity, i.e., the invariant Q is defined as

$$Q = \int_0^\infty I(q) q^2 \, dq \quad (2)$$

where q (scattering vector) $= (4\pi/\lambda_{LS}) \sin(\theta_{LS}/2)$ and $I(q)$ is the intensity of the scattered light at q.[21]

In the H_v mode the invariant Q_δ can be described by the mean-square optical anisotropy $\langle\delta^2\rangle$:

$$Q_\delta \propto \langle\delta^2\rangle \propto \phi_s(\alpha_r - \alpha_t)^2 \quad (3)$$

where ϕ_s is the volume fraction of spherulites, and α_r and α_t are the radial and tangential polarizabilities of spherulites, respectively. We constructed a plot of reduced invariant Q_δ/Q_δ^∞ vs time t with Q_δ^∞ being Q_δ at an infinitely long time of crystallization (up to full solidification of the melt).

Figure 6 shows the time variation of the invariant Q_δ/Q_δ^∞ taken for neat PLA and PLACN4 at 110 °C. The overall crystallization rate was determined from the slope Q_δ/Q_δ^∞ ($d(Q_\delta/Q_\delta^\infty)/dt$) in the crystallization region, as indicated by the solid line in Figure 6, and is plotted in Figure 7. It is clear that the overall crystallization rate increases in PLACN4, in comparison to the pristine PLA, as well as the rate increases in the case of PLACN4 for a particular T_c. The same trend is also observed over the wide range of T_c studied here. Here it should be mentioned that the equilibrium melting temperatures (T_m^0) of the PLACN4 and neat PLA are the same. The T_m^0's were measured by isothermal crystallization at various temperatures by carrying out a Hoffman−Weeks[22] plot as shown in Figure 8. Both PLACN4 and neat PLA show the same value of T_m^0 of

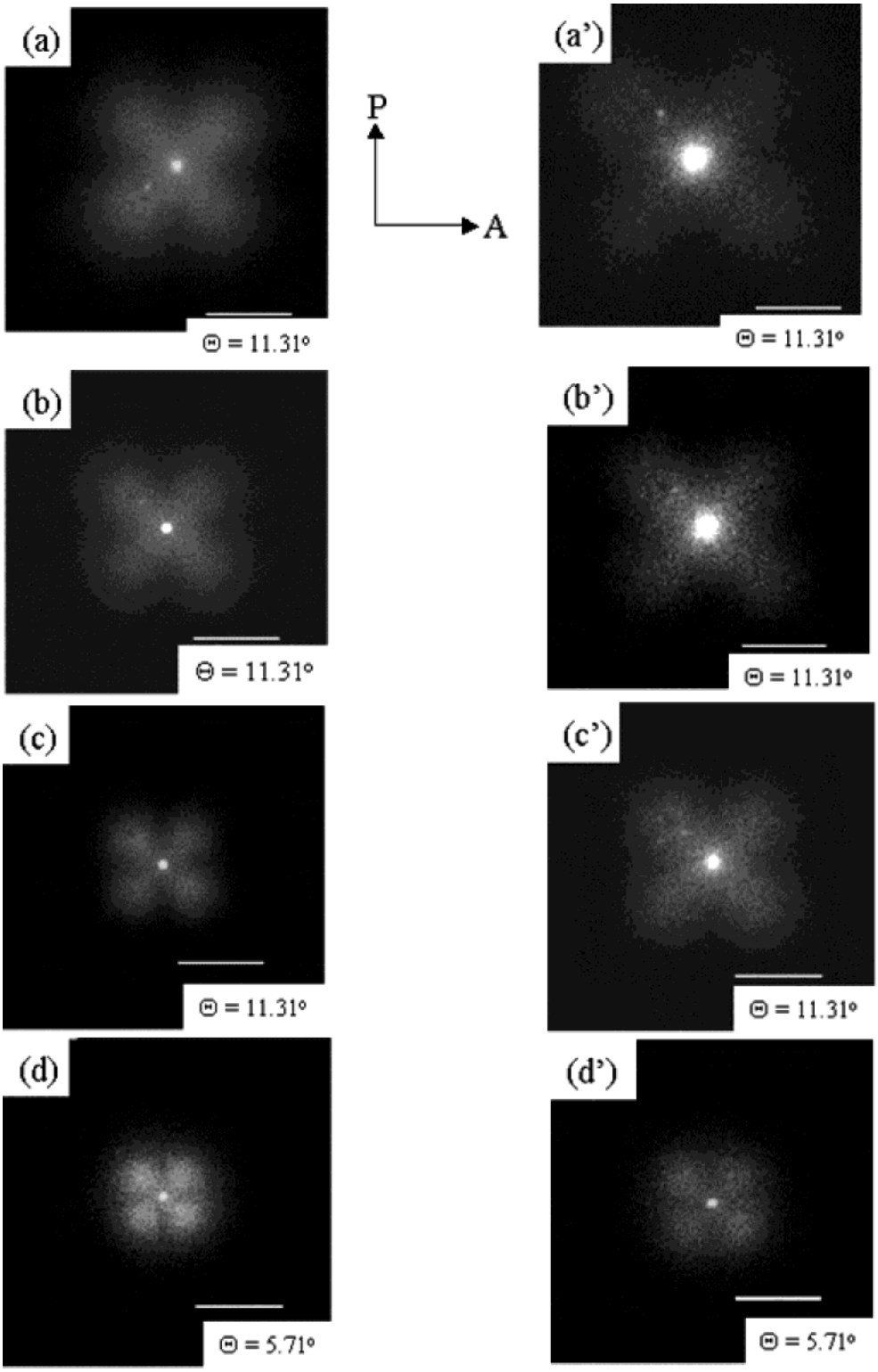

Figure 4. Changes in light scattering patterns of neat PLA (a−d) and PLACN4 (a′−d′) at various crystallization temperature under H_v modes: (a, a′) T_c = 90 °C; (b, b′) T_c = 100 °C; (c, c′) T_c = 110 °C; (d, d′) T_c = 120 °C.

179.54 °C, and that would nullify the effect of supercooling ΔT ($\equiv T_m^0 - T_c$) on the overall crystallization rate, linear growth rate, G, etc. The overall crystallization rate with T_c is a typical rate curve as usual for semicrystalline polymer.[23] However, the rate of PLACN4 is enhanced for every temperature of measurement, especially at higher T_c's. From the onset time t_0 we can estimate the induction time of the crystallization until start of crystallization. The observed value of t_0 at 110 °C was 74 s for pure PLA and 56 s for PLACN4. At all T_c measured here the t_0 value for PLACN4 is always lower than that of pure PLA. This reduction of t_0 in the case of PLACN4 is attributed to the presence of MMT particle as a nucleating agent.

The typical example of the time variation of the diameter of the spherulite D for neat PLA and PLACN4 at higher T_c's is shown in Figure 9a, and the linear growth rate G ($= {}^1/_2(dD/dt)$) of spherulite is summarized in Figure 9b. For both neat PLA and PLACN4, G decreases with increasing T_c in the temperature range

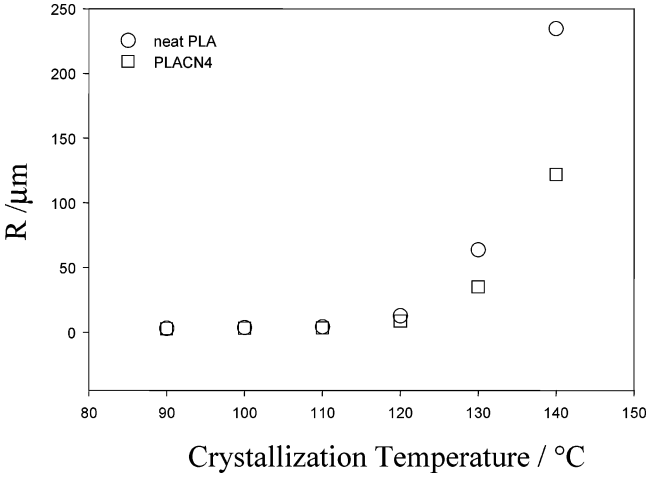

Figure 5. T_c dependence of the spherulite radius, R_s, of neat PLA and PLACN4.

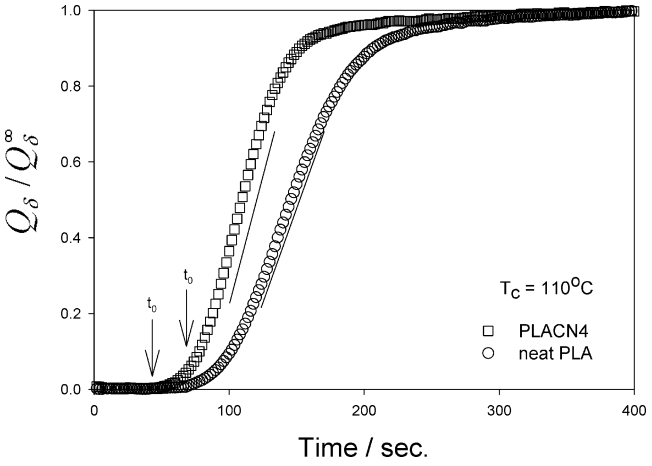

Figure 6. Time variation of reduced invariant Q_δ/Q_δ^∞ during isothermal crystallization at quiescent state at T_c = 110 °C. The solid line represents the slope (overall crystallization rate).

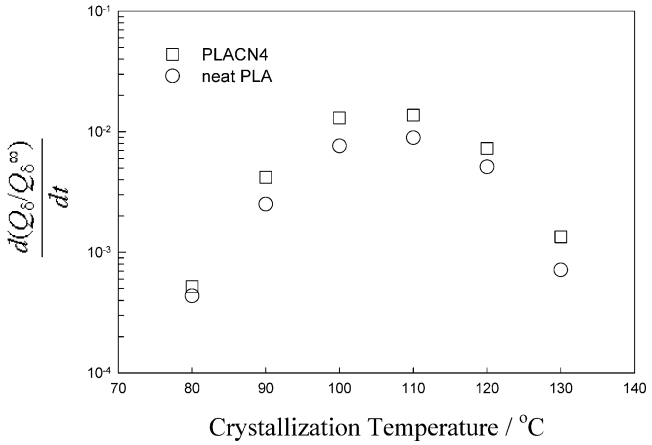

Figure 7. T_c dependence of the overall crystallization rate of neat PLA and PLACN4.

120−140 °C. However, for PLACN4, G shows little higher value compared to that of neat PLA.[24] This behavior may be due the little low molecular weight of matrix in PLACN4. This observation indicates that the dispersed clay particles have almost no effect on the acceleration of G during the crystallization of PLACN4. This observation suggests that the diffuse rate of bulk PLA molecules is not enhanced with the addition of C_{18}-MMT for every temperature of measurement, so that

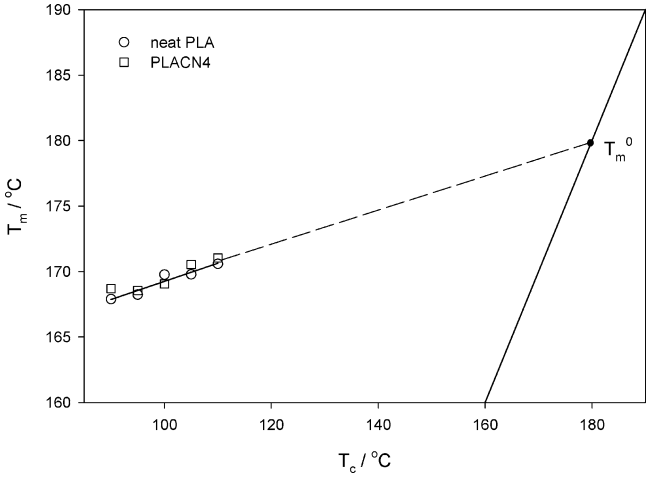

Figure 8. T_m vs T_c (Hoffman−Weeks) plots of neat PLA and PLACN4.

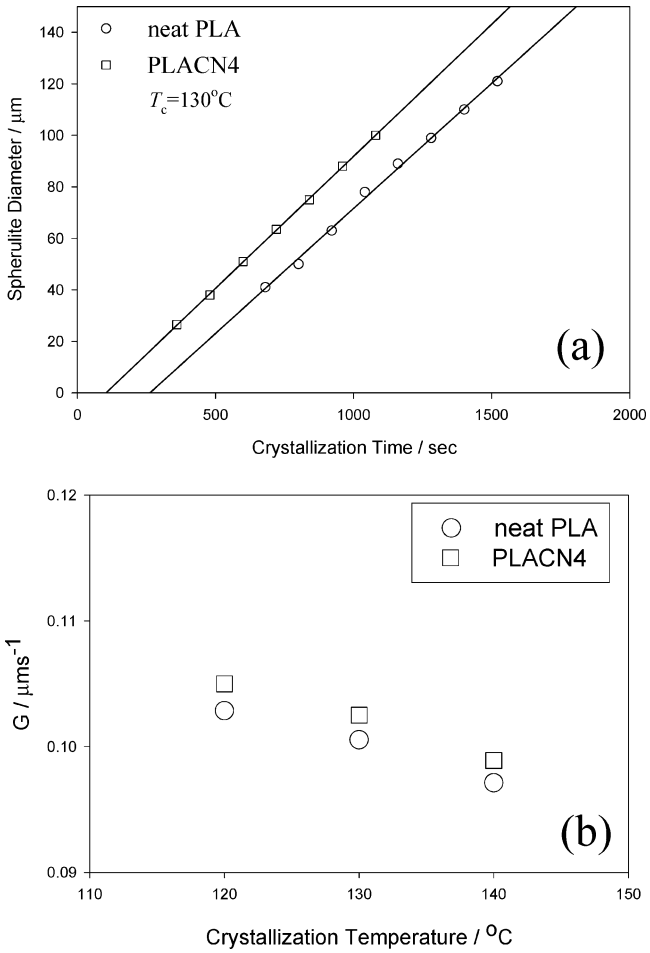

Figure 9. (a) Spherulite diameter as a function of crystallization time at T_c = 130 °C and (b) linear growth rate of neat PLA and PLACN4 as a function of T_c.

the overall crystallization rate is affected only by nucleation of the MMT particles.[25]

From Figure 10, the number of heterogeneous nuclei N can be estimated from a rough approximation. That is, all the spherulites were of identical size, the primary nucleation density of the spherulites, i.e., the number of heterogeneous nuclei N, was estimated by[25]

$$N = ({}^3/_4\pi)R_m^{-3} \quad (4)$$

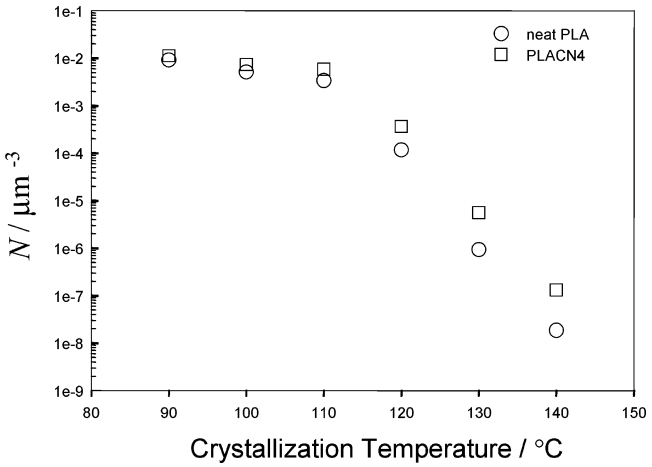

Figure 10. Nucleation density N of neat PLA and PLACN4 as a function of T_c.

where R_m is the maximum radius of the spherulite ($\equiv R_s$), i.e., the attainable radius before impingement. The calculated value of N at 130 °C was $9.3 \times 10^{-7}\ \mu m^{-3}$ for neat PLA and $55.7 \times 10^{-7}\ \mu m^{-3}$ for PLACN4. The time variation of the volume fraction of the spherulites increases in proportion to NG^3 ($\cong$ overall crystallization rate). This fact suggests that the overall crystallization rates of the PLACN4 at high temperature ($T_c = 130$ °C) are about half order of magnitude higher than that of matrix PLA without C_{18}-MMT. The difference of N between pure PLA and PLACN4 at $T_c = 130$ °C is higher than that at low T_c. This suggests that the PLACN4 exhibit a heterogeneous nucleation kinetics, which depends on more originating from the well-dispersed MMT particles in the matrix at high temperature. Here, we should mention that the spherulites of PLACN4 have a lower ordering than that of neat PLA due to the dispersed MMT particles in the spherulites. Hence, the aggregation of MMT particles, which is not nucleated during crystallization, exists inside the spherulite, and then the occurrence of the regular orientation of lamella stacks inside the spherulite may be disrupted.

Conclusions

In this paper, we have described the detailed crystallization behavior and morphology of pure PLA and one representative PLA/C_{18}-MMT nanocomposite. Both neat PLA and nanocomposite spherulites exhibited negative birefringence, but ordering of spherulites is much higher in the case of pure PLA. The overall crystallization rate of neat PLA increases after nanocomposite preparation with C_{18}-MMT, but it has no influence on the linear growth rate of pure PLA. These behaviors indicate dispersed MMT particles act as a nucleating agent for PLA crystallization in the nanocomposite.

Acknowledgment. Dr. S. Sinha Ray thanks the Japan Society for the Promotion of Science (JSPS) for financial support (Grant P02152). We express our appreciation to the reviewers for their constructive and meticulous assessment of the manuscript.

References and Notes

(1) Drumright, R. E.; Gruber, P. R.; Henton, D. E. *Adv. Mater.* **2000**, *12*, 1841.
(2) Kim, S. H.; Han, Y.-K.; Kim, Y. H.; Hong, S. I. *Macromol. Chem.* **1991**, *193*, 1623. Kricheldorf, H. R.; Serra, A. *Polym. Bull.* **1985**, *14*, 497. Kricheldorf, H. R.; Berl, M.; Scharngal, N. *Macromolecules* **1988**, *21*, 286. Nijenhuis, A. J.; Grijpma, D. W.; Pennings, A. J. *Macromolecules* **1992**, *25*, 6419.
(3) Lunt, J. *Polym. Degrad. Stab.* **1998**, *59*, 145.
(4) Grijpma, D. W.; Pennings, A. J. *Macromol. Chem. Phys.* **1994**, *195*, 1649. Perego, G.; Cella, G. D.; Bastioli, C. *J. Appl. Polym. Sci.* **1996**, *59*, 37. Sinclair, R. G. *J. Macromol Sci., Pure Appl. Chem.* **1996**, *A33*, 585. Tsuji, H.; Ikada, Y. *J. Appl. Polym. Sci.* **1998**, *67*, 405. Martin, O.; Averous, L. *Polymer* **2001**, *42*, 6209.
(5) Sinha Ray, S.; Okamoto, M. *Prog. Polym. Sci.*, in press. Biswas, M.; Sinha Ray, S. *Adv. Polym. Sci.* **2001**, *155*, 167. Alexander, M.; Dubois, P. *Mater. Sci. Eng., R* **2000**, *28*, 1. Giannelis, E. P.; Krishnamoorti, R.; Manias, E. *Adv. Polym. Sci.* **1999**, *138*, 107. LeBaron, P. C.; Wang, Z.; Pinnavaia, T. J. *Appl. Clay. Sci.* **1999**, *15*, 11. Giannelis, E. P. *Adv. Mater.* **1996**, *8*, 29.
(6) Sinha Ray, S.; Maiti, P.; Okamoto, M.; Yamada, K.; Ueda, K. *Macromolecules* **2002**, *35*, 3104.
(7) Sinha Ray, S.; Yamada, K.; Okamoto, K.; Okamoto, M. *Nano Lett.* **2002**, *2*, 423. Sinha Ray, S.; Yamada, K.; Okamoto, M.; Ogami, A.; Ueda, K. *Compos. Interfaces*, in press.
(8) Sinha Ray, S.; Yamada, K.; Okamoto, M.; Ueda, K. *Nano Lett.* **2002**, *2*, 1093. Sinha Ray, S.; Yamada, K.; Okamoto, M.; Ueda, K. *Polymer* **2003**, *44*, 857.
(9) Sinha Ray, S.; Yamada, K.; Ogami, A.; Okamoto, M.; Ueda, K. *Macromol. Rapid Commun.* **2002**, *23*, 943. Sinha Ray, S.; Yamada, K.; Okamoto, M.; Ogami, A.; Ueda, K. *Chem. Mater.* **2003**, *15*, 1456.
(10) Sinha Ray, S.; Yamada, K.; Okamoto, M.; Ueda, K. *Macromol. Mater. Eng.* **2003**, *288*, 203.
(11) Fujimoto, Y.; Sinha Ray, S.; Okamoto, M.; Yamada, K.; Ogami, A.; Ueda, K. *Macromol. Rapid Commun.* **2003**, *24*, 457.
(12) Nam, P. H.; Maiti, P.; Okamoto, M.; Kotaka, T.; Hasegawa, N.; Usuki, A. *Polymer* **2001**, *42*, 9633.
(13) Fisher, E. W.; Sterzel, H. J.; Wegner, G. *Kolloid Z. Z. Polym.* **1973**, *25*, 980.
(14) Before starting each experiment, the Linkam hot stage was calibrated using water and indium as standards.
(15) Kubo, H.; Sato, H.; Okamoto, M.; Kotaka, T. *Polymer* **1998**, *39*, 501.
(16) Okamoto, M.; Kubo, H.; Kotaka, T. *Polymer* **1998**, *39*, 3135.
(17) Hoogsteen, W.; Postema, A. R.; Pennings, A. J.; TenBrinke, G.; Zugenmaier, P. *Macromolecules* **1990**, *23*, 634. Kobayashi, J.; Asahi, T.; Ichiki, M.; Okikawa, A.; Suzuki, H.; Watanabe, T.; Fukaka, E.; Shikimami, Y. *J. Appl. Phys.* **1995**, *77*, 2957. Brizzolara, D.; Cantow, H. J.; Diederichs, K.; Keller, E.; Domg, A. J. *Macromolecules* **1996**, *29*, 191.
(18) Eling, B.; Gogolewski, S.; Pennings, A. J. *Polymer* **1982**, *23*, 1587. Vasanthakumari, R.; Pennings, A. J. *Polymer* **1993**, *24*, 175.
(19) Nam, J. Y.; Kacomatsu, S.; Saito, H.; Inoue, T. *Polymer* **2002**, *43*, 2101.
(20) Stein, R. S.; Rhodes, M. B. *J. Appl. Phys.* **1960**, *31*, 1873.
(21) Okamoto, M.; Inoue, T. *Polymer* **1995**, *36*, 2736.
(22) Martuscelli, E.; Silvestre, S.; Abate, G. *Polymer* **1982**, *23*, 229.
(23) Okamoto, M.; Shinoda, Y.; Kinami, N.; Okuyama, T. *J. Appl. Polym. Sci.* **1995**, *57*, 1055. Moore, E. P., Jr. *Polypropylene Handbook;* Hanser/Gardner: Cincinnati, OH, 1996.
(24) Little low molecular weight of PLA matrix in PLACN4 is the main reason to observe little high spherulites growth rate in case of PLACN4 because radial growth rate of the spherulites is inversely proportional to the degree of polymerization.
(25) Maiti, M.; Nam, P. H.; Okamoto, M.; Hasegawa, N.; Usuki, A. *Macromolecules* **2002**, *35*, 2042.

MA034623J